Fluid Dynamics Research

The Japan Society of Fluid Mechanics

PAPER

Numerical simulation of head-on collision of two coaxial vortex rings

To cite this article: M Cheng *et al* 2018 *Fluid Dyn. Res.* **50** 065513

View the article online for updates and enhancements.

This content was downloaded from IP address 103.21.125.76 on 14/01/2020 at 17:09

IOP Publishing | The Japan Society of Fluid Mechanics Fluid *Dynamics* Research

Fluid Dyn. Res. **50** (2018) 065513 (24pp) https://doi.org/10.1088/1873-7005/aae54b

Numerical simulation of head-on collision of two coaxial vortex rings

M Cheng[1,3], **J Lou**[1] **and T T Lim**[2]

[1] Institute of High Performance Computing, Agency for Science, Technology and Research (A*STAR), 1 Fusionopolis Way, #16-16 Connexis, Singapore 138632, Singapore

[2] Department of Mechanical Engineering National University of Singapore, Singapore 117576, Singapore

E-mail: chengm@ihpc.a-star.edu.sg, loujing@ihpc.a-star.edu.sg and mpelimtt@nus.edu.sg

Received 15 December 2017, revised 24 July 2018
Accepted for publication 1 October 2018
Published 9 November 2018

Communicated by Yasuhide Fukumoto

Abstract

Past experimental and numerical studies show that when two identical circular vortex rings of moderate Reynolds number collide head-on, vortex ringlets are generated around the circumference of the primary vortex rings and propagated radially outward through self-induction. Here, we show that dissimilarity in vortex core sizes between two colliding rings, despite having the same circulation, can significantly affect the outcome of the collision. This finding may help to explain the asymmetry in vortex ringlets formation observed in some of the experimental studies, which could be due to imperfections in vortex ring generators. The study was carried out by using a lattice Boltzmann method for the Reynolds number range of $500 \leqslant Re_{\Gamma} \leqslant 2000$. Our simulations show that in the absence of azimuthal perturbations on primary vortex rings, dissimilar core sizes between the two rings leads to unequal induced velocity on each other and hence unequal rates of radial expansion. This scenario sets up a condition that enables the thicker-core vortex ring (slower moving) to 'slip-over' a thinner-core ring (faster moving). Thereafter, the rings contract radially due to mutual induction as they propagate away from each other in opposite direction. For a sufficiently low Reynolds number, the 'slip-over' process does not take place due to the combined effect of lower momentum of the approaching rings and a more dominate effect of viscosity. Under this circumstance, the two primarily vortex rings remain in constant proximity during the collision, and the ensuing cross diffusion of vorticity of

[3] Author to whom any correspondence should be addressed.

 © 2018 The Japan Society of Fluid Mechanics and IOP Publishing Ltd Printed in the UK

opposite sign at the collision 'plane' eventually leads to the 'demise' of the vortex rings. However, in the presence of an azimuthal perturbation at a moderate Reynolds number, the attempted slip-over by a thicker-core vortex ring causes a realignment of their azimuthal perturbations. This leads to the reorientation of resulting vortex ringlets, which travel outward in directions that are inclined to the plane of collision. This inclination angle increases with initial core size ratio, with a near zero inclination angle for the case of identical vortex rings.

Keywords: vortex ring, viscous fluid, vortex reconnection, lattice Boltzmann method

(Some figures may appear in colour only in the online journal)

1. Introduction

Vortices are omnipresent in nature and a hallmark of unsteady fluid flow such as boundary-layer separation, turbulent jets, wall-bounded turbulent and viscous flows (Lugt 1983, Saffman 1992, Kelso *et al* 1996, Pullin and Saffman 1998). Of all the vortices in nature, vortex rings are perhaps the simplest and most compact. They are easily generated in a laboratory and have been a subject of much research for more than a century (Shariff and Leonard 1992, Meleshko 2010). The research includes the formation and characteristics of an isolated vortex ring, a vortex ring interacting with another ring (henceforth referred to as ring–ring interaction) and a vortex ring interacting with a solid wall (henceforth referred to as ring-wall interaction). One of the key motivations in these studies stems from the quest to better understand intrinsic flow phenomena which occur in turbulent flows, such as vortex stretching, vortex instability and vortex reconnection. And vortex rings provide a unique platform to study these phenomena as they can be forced to interact in a predetermined manner. Besides fundamental interests, vortex ring interactions have been observed in various technological situations and applications (Shariff and Leonard 1992, Konstantinov 1994, Lim and Nickels 1995, Lim 1997a, 1998, Bourne *et al* 2017).

In a laboratory, one of the often studied ring–ring interactions is that between two coaxial vortex rings (Meleshko 2010). The interaction can be broadly divided into two categories: passage interaction and collision interaction. In the passage interaction, two vortex rings travel coaxially in the same direction. For a specific case of two circular vortex rings of equal size and strength, their mutual induction causes the front vortex ring to expand radially and slow down, and the rear ring to contract and speed up. The rear ring eventually slips through the center of the front ring in a process commonly referred such as vortex leapfrogging (Yamada and Matsui 1978, Lim 1997b, Mariani and Kontis 2010, Borisov *et al* 2014, Cheng *et al* 2015). With careful control of the generating condition, two slip-throughs have been reported in literatures before the rings finally merged into a single and larger ring. On the other hand, collision interaction involves two coaxial vortex rings approaching each other head-on. For a specific case of two circular vortex rings of equal strength and size, Chu *et al* (1995) broadly divide the collision process into three stages, namely free-traveling stage, vortex stretching stage and viscous dissipation dominant stage. Free-traveling stage occurs when the separation distance between the two rings is sufficiently large (usually more than one ring diameter) that their mutual induction is minimal. Vortex stretching stage happens when the vortex rings are in closed proximity, and their mutual induction causes both of them

to expand radially and slow down. Viscous dissipation stage occurs in the last phase of the interaction when viscous diffusion dominates. At a sufficiently low Reynolds number, vortex stretching merely intensifies the vorticity of two vortex rings and speeds up their dissipation through viscous diffusion. At a moderately high Reynolds number, vortex stretching is often accompanied by vortex instability in the form of azimuthal waves around the circumference of the rings (Lim and Nickels 1992). These wavy instabilities grow until they touch each other at the locations of maximum inward displacement. The vortex reconnection process that follows at the regions of contact eventually leads to the formation of smaller rings (henceforth referred to as vortex ringlets). The resulting vortex ringlets then propagate, through self-induction, away from the center of the primary rings until their vorticity is dissipated through viscous diffusion (Lim and Nickels 1992). In the case of two vortex rings with unequal initial circulation, the past study shows that the head-on collision resulted in the faster traveling vortex ring 'slipping' through the center of the slower moving ring (Inoue *et al* 2000). In the present study, our attention is focused primarily on head-on collision between two coaxial vortex rings.

One of the earliest studies on the head-on collision between two identical circular vortex rings was carried out by Oshima (1978) in air using smoke visualization technique. She observed that when the two rings were in closed proximity, vortex stretching due to their radial expansion causes the smoke cross-sections of the rings to deform from a circular shape to an elongated head with a long trailing tail. She also noticed that at low Reynolds number, the smoke rings remained close to each other after they had expanded to several times their original radii. It is likely that what she had observed in the final stage of the collision is merely a remnant of the demised vortex rings after the vorticity has been smoothed out by viscous diffusion, leaving behind only smoke trail. However, she found that above a certain critical velocity or Reynolds number, the vortex filaments developed wavy instability, followed by cross-linking between them which resulted in the generation of small sub-rings around the circumference that resembles a necklace. These sub-rings subsequently diffused rapidly through viscous diffusion. In a later study, Lim and Nickels (1992) conducted similar experiment in water using two different color dyes. They found that radial expansion of the rings during the early stage of the collision follows an inviscid prediction (Gurzhii and Konstantinov 1989) reasonably well, and the resulting vortex ringlets that formed through vortex reconnection of azimuthal instability consists of segments or 'DNA' of the 'parent' rings.

The above flow visualization studies, while displaying fascinating and complex flow topology, were unable to provide quantitative data. This shortcoming led many researchers to turn to computational methods as an alternative tool to unravel physics of fluid during the collision. Stanaway *et al* (1988) were among the earliest researchers to conduct numerical studies on the head-on collision of two viscous vortex rings by solving the Navier–Stokes (NS) equations in an unbounded domain using a spectral method. Their result revealed the head-tail structure at the Reynolds numbers of about 350 and 1000. Using combined experimental and numerical approach, Chu *et al* (1995) studied the head-on collision of two coaxial vortex rings in an incompressible viscous fluid for Reynolds number ranging from 400 to 2700. Their results, which were discussed briefly above, broadly divide the collision into three stages prior to the breakdown of vortex rings, i.e. free-traveling stage, vortex-stretching stage, and viscous dissipation dominance stage. Mansfield *et al* (1999) also studied the head-on collision of two coaxial vortex rings in three-dimensions using a Lagrangian large eddy simulation approach. Their scheme combines a three-dimensional, adaptive, viscous, vortex element method with a dynamic eddy viscosity model of the sub-filter scale stresses, and their method can capture several distinctive flow phenomena reported by Lim and Nickels (1992), including the formation of vortex ringlets. They further show that the final outcome of the collision is dependent on the alignment of the initial azimuthal perturbation imposed on

each of the rings. In a more recent study, Guan *et al* (2016) numerically simulated head-on collision of two vortex rings in an inviscid fluid using a second order finite volume scheme. They showed that their scheme can capture some of the flow features during the collision including turbulent breakdown into small-scale structures.

The head-on collision between two identical vortex rings has been studied extensively in the past; more so numerically than experimentally because of relative ease of implementing head-on collision computationally. In a laboratory, imperfection in vortex ring generators can sometimes lead to asymmetry in the vortex ringlets formation even when the approaching rings are physically aligned prior to the collision. The asymmetry is probably caused by dissimilarity in core size/circulation of the colliding vortex rings. But exactly how the dissimilarity dictates the outcome of the collision is not entirely clear as this issue has not been thoroughly investigated in the past. The present study is motivated by our desire to address the above mentioned issue and to get an insight into this intrinsically fascinating problem. Also, we believe the findings from the present investigation are relevant to the study two opposite impinging circular jets where ring-like vortex structures of unequal circulation/core size are likely to coexist and interact. Here, we focus our attention on how dissimilarity in the vortex core size between two colliding vortex rings affects the outcome of the collision. A related study of two colliding vortex rings of unequal circulation, in the absence of azimuthal instability, has been conducted previously by Inoue *et al* (2000), but the study offers little insight into the actual vortex interaction. An added benefit of the present numerical study is that it provides quantitative data, such as temporal variation of core center vorticity, kinetic energy (KE) and enstrophy in the fluid system that would have been difficult to obtain experimentally. These quantitative results have not been previously published in literature. Here, we use lattice Boltzmann method (LBM) for the investigation; this method has developed into an alternative computational fluid dynamics approach to simulate vortex rings interaction (Chen and Doolen 1998, Cheng *et al* 2010).

The paper is organized as follows. In section 2, the computational setup is outlined together with a brief description of the LBM and relevant initial and boundary conditions. The code is validated by comparing the LBM results with the corresponding experimental results for the head-on collision between two identical circular vortex rings. Section 3 presents the numerical results of the evolution of two colliding vortex rings with respect to changes in the core size ratio and Reynolds number. The influence of azimuthal perturbation on the outcomes of the collision is also discussed. The paper ends with conclusions in section 4.

2. Computational Setup

2.1. Flow configuration

We consider two coaxial vortex rings (V_1 and V_2) approaching each other by self-induction in an incompressible viscous fluid. The rings have an identical initial circulation Γ_0, but different core sizes σ_{10} and σ_{20}. The separation distance between the rings is set initially at s_0, as shown in figure 1. The flow is governed by the continuity and NS equations

$$\nabla \cdot \mathbf{u} = 0, \tag{1}$$

$$\frac{\partial \mathbf{u}}{\partial t} + (\mathbf{u} \cdot \nabla)\mathbf{u} = -\frac{1}{\rho}\nabla p + \nu \nabla^2 \mathbf{u}, \tag{2}$$

where $\mathbf{u} = (u, v, w)$ is the velocity, t is the time, p is the pressure, ρ and ν are the density and the kinematic viscosity of fluid, respectively.

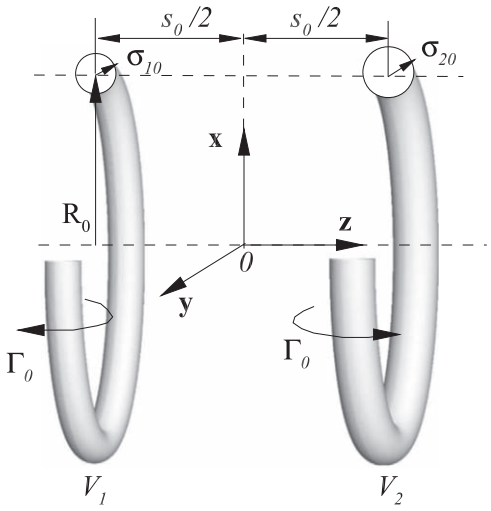

Figure 1. Schematics of the geometry for two vortex rings approaching each other.

The ring is initially placed at the position $(x_0, y_0, \pm z_0) = (0, 0, \pm s_0/2)$. The computational domain is $l_x \times l_y \times l_z$, where l_x, l_y and l_z are the dimensions of the domain in the x, y and z directions, respectively. The domain is discretized by a uniform lattice.

The initial vorticity distribution of the vortex ring is assigned by a Gaussian function (Orlandi and Verzicco 1993, Cheng *et al* 2010),

$$\mathbf{\Omega}_0(\sigma) = \frac{\Gamma_0}{\pi\sigma_0^2} \mathrm{e}^{-\left(\frac{\sigma}{\sigma_0}\right)^2} \mathbf{e}_\Gamma, \tag{3}$$

for which the velocity distribution around the ring can be written as

$$\mathbf{u}_0(\sigma) = \frac{\Gamma_0}{2\pi\sigma}[1 - \mathrm{e}^{-(\sigma/\sigma_0)^2}]\mathbf{e}_T, \tag{4}$$

where σ is the radial distance from the center of vortex core, σ_0 is the initial core radius, $\mathbf{e}_\Gamma$ and $\mathbf{e}_T$ are the unit vector along the vortex line and the unit tangent vector to circulation circles about the ring core, respectively. The periodic conditions are used at the boundaries whose normal vector is parallel to z-axis, while the constant-pressure boundary conditions are imposed at the rest of boundaries.

Dimensionless variables are defined according to

$$\mathbf{R} = \frac{\mathbf{r}}{R_0}, \quad T = \frac{\Gamma_0 t}{R_0^2}, \quad \mathbf{\Omega} = \frac{\boldsymbol{w} R_0^2}{\Gamma_0}, \quad Re_\Gamma = \frac{\Gamma_0}{\nu}, \quad \eta = \frac{\sigma_{20}}{\sigma_{10}}, \tag{5}$$

where $\mathbf{r} = (x, y, z)$ is the spatial vector in the Cartesian coordinates system, $\boldsymbol{w} = (\omega_x, \omega_y, \omega_z)$ is the vorticity, η is the vortex core radius ratio between ring V_1 and ring V_2.

The velocity and vorticity at time t obtained by the computation can be used to calculate the global KE E_u and enstrophy E_Ω, namely

$$E_u = 0.5 \int\int\int_v \mathbf{u} \cdot \mathbf{u} \mathrm{d}v. \tag{6}$$

$$E_\Omega = 0.5 \int\int\int_v \mathbf{\Omega} \cdot \mathbf{\Omega} \mathrm{d}v. \tag{7}$$

2.2. Numerical method

The numerical approach used to solve equations (2.1) and (2.2) is the LBM which is the same as the one used in the (Cheng *et al* 2010). The code has been continuously developed, refined and applied to vortex dynamics in the last 10 years by the group (Cheng and Luo 2007 and Cheng *et al* 2010, 2014, 2015, 2016). Interested readers are referred to Cheng *et al* (2010) for the implementation details.

2.3. Validation

The results of various validation of the code have been reported previously, and demonstrated a capability to accurately predict complicated vortex ring motion (Cheng *et al* 2010, 2014, 2015, 2016). To verify the present numerical model, using the grid density $R_0 = 80\Delta x$, we simulate the head-on collision of two identical circular vortex rings which have been studied experimentally (Lim and Nickels 1992, Chu *et al* 1995). Our previous experience indicated that this resolution is sufficient for the flow at $Re_\Gamma < 3000$ (Cheng *et al* 2016). The comparison in figure 2 of the numerical results obtained by the present method and the experimental flow visualization at $Re_\Gamma = 1500$ (Chu *et al* 1995) show that our simulations can capture the salient features of expanding vortex rings in the early stage of collision. The agreement is further established by quantitative comparison of the trajectories of the vorticity centers of the ring in upper half of the x−z plane ($x \geqslant 0$) as shown in figure 3. The center of a vortex core is defined as follows:

$$x_c = \int\int x\Omega_y \mathrm{d}x\mathrm{d}z / \int\int \Omega_y \mathrm{d}x\mathrm{d}z, \tag{8}$$

$$z_c = \int\int z\Omega_y \mathrm{d}x\mathrm{d}z / \int\int \Omega_y \mathrm{d}x\mathrm{d}z. \tag{9}$$

Clearly, our numerical results for the early stage of collision agree quantitatively with the experimental measurement of Chu *et al* (1995).

In our numerical computation, there is a numerical perturbation of four-fold symmetry due to the geometry shape of computational domain, but its influence is too small to affect vortex ring behavior during collision at low Reynolds number $Re_\Gamma \leqslant 2000$ even after a very long computational time (Verzicco and Orlandi 1994, Cheng *et al* 2010). Even at a larger Reynolds number, the rings still remain close parallel to each other as time progresses. However, it is worth noting that topology changes due to reconnection of vortex filaments, which was observed in experiment, could not be achieved in the numerical simulation. In a real flow, azimuthal instability (Widnall and Sullivan 1973, Widnall *et al* 1974) develops around the circumference of a vortex ring sometime after it is formed. This instability grows with time and influences the outcome of vortex ring collision, especially during the later stages. To better reflect the dynamics of real vortex rings, an initial perturbation is imposed around the circumference of the ring in the numerical simulations (Bergdorf *et al* 2007, Verzicco and Orlandi 1994, Mansfield *et al* 1999, Cheng *et al* 2016). To provide further verification of our numerical scheme, we simulate the evolution of head-on collision between two identical vortex rings with an initial perturbation over a much longer dimensionless time. This flow configuration is similar to the experiment conducted by Lim and Nickels (1992). In our simulation, the perturbation is introduced into initial velocity in the azimuthal direction by

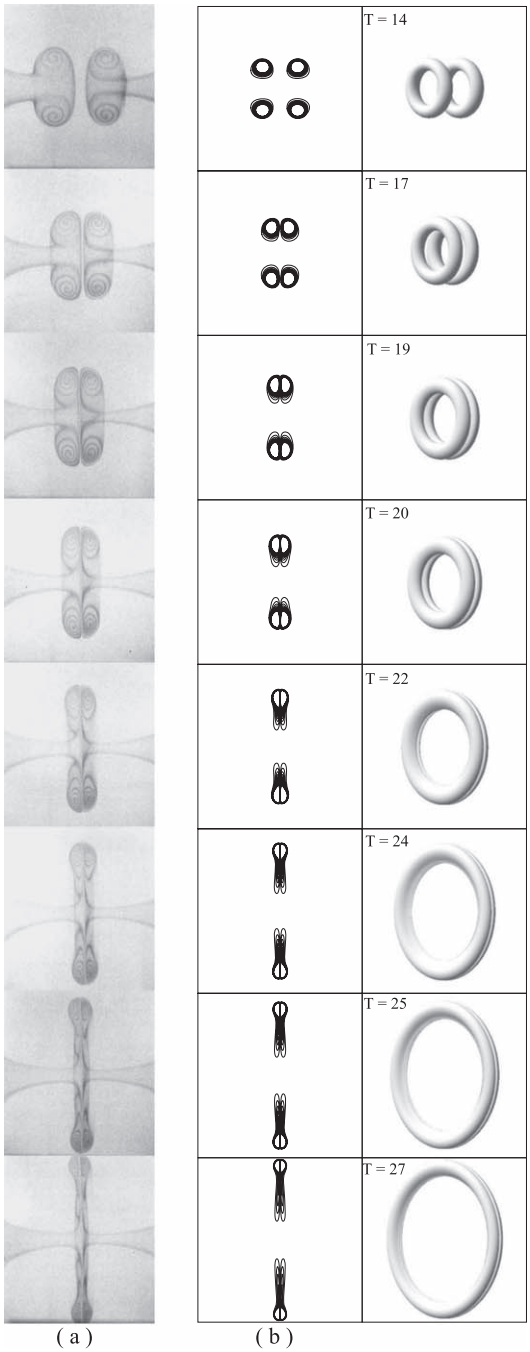

Figure 2. Evolution of the vortex ring patterns for $Re_\Gamma = 1500$, $\sigma_{01} = \sigma_{02} = 0.18R_0$ and $s_0 = 8R_0$. Comparison between the experimental visualization (Chu *et al* 1995) and the present computational results (contours are plotted in the range of $|\Omega_y| \leqslant 1$ with a level interval of $\Delta\Omega_y = 0.1$, and the iso-surface is $||\boldsymbol{\Omega}|| = 1$). Reproduced with permission from Chu *et al* (1995). © 1995 Cambridge University Press.

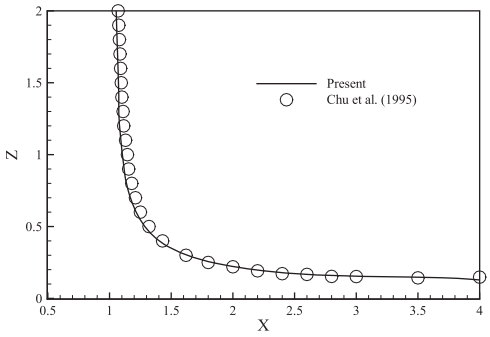

Figure 3. Trajectories of the loci of the vortex-ring core for $Re_\Gamma = 1500$. The line represents the results of the present LBM simulation and the symbols represent the experimental data (Chu *et al* 1995).

displacing the axis of the vortex core using a sine-wave perturbation as used in other numerical simulations (Verzicco and Orlandi 1994, Mansfield *et al* 1999, Cheng *et al* 2016). The bending wave perturbation is specified in terms of its amplitude A_m and wavenumber N. Figure 4 shows a comparison of the results obtained by the present method and the experimental flow visualization for two circular vortex rings at $Re_\Gamma = 1600$ (Lim and Nickels 1992). It can be seen that important flow features during the collision are portrayed in our simulation. Specifically, as the two vortex rings approach each other, their mutual induction causes them to expand radially and slow down. After each of the rings has expanded to about four times its initial diameter, flow instability in the form of azimuthal waviness begins to develop and grows with time. When the opposing 'wavy' vortex filaments eventually come in contact with each other, vortex reconnection at the regions of contact leads to the formation of smaller sub-rings or vortex ringlets with each half of the ringlet contributed by the 'parent' rings. Once generated, the ringlets propagate radially outward from the center of the primary rings and their vorticity is eventually dissipated via viscous diffusion. These observations are consistent with the experimental findings reported by Lim and Nickels (1992).

In this paper, unless otherwise stated, a sufficiently large computational domain $l_x \times l_y \times l_z = 20R_0 \times 20R_0 \times 6R_0$ and the resolution $R_0 = 80\Delta x$ are adopted for the subsequent computations.

3. Results and discussion

Here, the results of the computation are presented for a range of parameters, namely Reynolds numbers (Re_Γ) ($500 \leqslant Re_\Gamma \leqslant 2000$) and core radius ratios (η) ($1 \leqslant \eta \leqslant 1.5$). The initial core radius of the vortex V_1 is fixed at $\sigma_{01} = 0.1R_0$ and the initial separation distance between the two rings is set at $s_0 = 2R_0$, while the other parameters (η and Re_Γ) are systematically varied. We first present the results of two colliding vortex rings without initial azimuthal perturbations, and follow by the collision with initial azimuthal sinusoidal perturbations.

3.1. Collision between two identical vortex rings

Although numerical simulation of head-on collision of two identical has been reported in the past, the results are presented here for completeness and for purpose of comparison with the

Figure 4. The head-on collision between two identical vortex rings for $Re_\Gamma = 1600$, $\sigma_{01} = \sigma_{02} = 0.1R_0$ and $s_0 = 2R_0$. (a) The experimental flow visualization (Lim and Nickels 1992), and (b) the present numerical simulation with a perturbation $A_m = 0.05$ and $N = 18$ for different time instances. Reprinted by permission from Macmillan Publishers Ltd: Nature (Lim and Nickels 1992), Copyright (1992).

corresponding results with unequal core sizes. Figure 5 presents the evolution of two colliding vortex rings (in the form of iso-surface of constant vorticity) at $Re_\Gamma = 500$ and 1000. One obvious feature of the collision process is the radial expansion of the vortex rings while maintaining axial symmetry. This behavior is also captured quantitatively in figure 6 where it can be observed that the rate of radial expansion during the initial stage of the collision is small $0 < T < 3$ since the rings are relatively far apart from each other and mutual interaction between them is small. When in close-proximity, the expansion rate of the rings accelerates

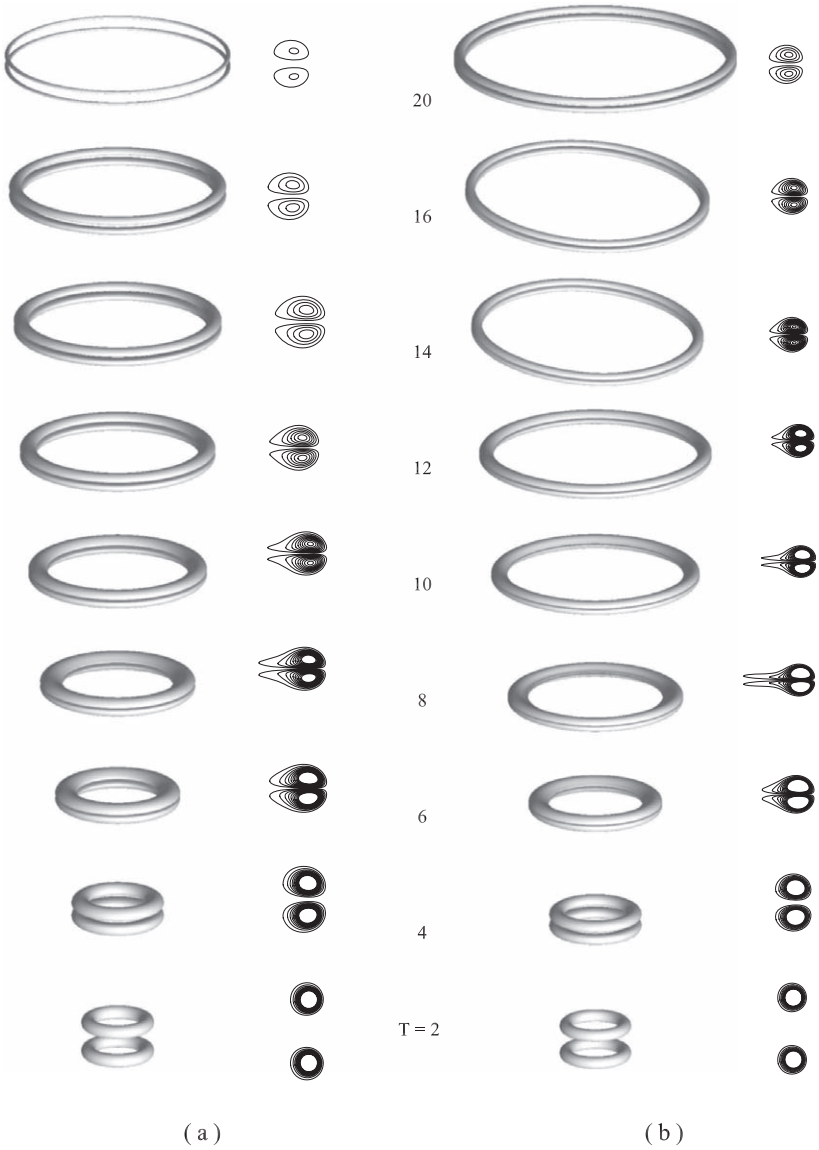

Figure 5. Development of flow structure (represented by the iso-surface of constant vorticity $||\boldsymbol{\Omega}|| = 1.0$) and vorticity contours in the $y = 0$ plane of symmetry during the head-on collision between two identical vortex rings at different Reynolds numbers (contours are plotted in the range of $|\Omega_y| \leqslant 5$ with a level interval of $\Delta\Omega_y = 0.5$). (a) $Re_\Gamma = 500$ (b) $Re_\Gamma = 1000$.

until it reaches a peak value at around $T = 7$ before it gradually tapers off due to continual loss of vorticity through viscous diffusion. This behavior applies to all the Reynolds number considered here except that higher Reynolds number produces higher rate of radial expansion and therefore higher peak value. The corresponding changes in core center vorticity (Ω_x) and enstrophy in the fluid system (E_Ω) are illustrated in figures 7(a) and (b) for different *Re*. Looking at each plot separately, it is of interest to note from figure 7(a) that for a fixed

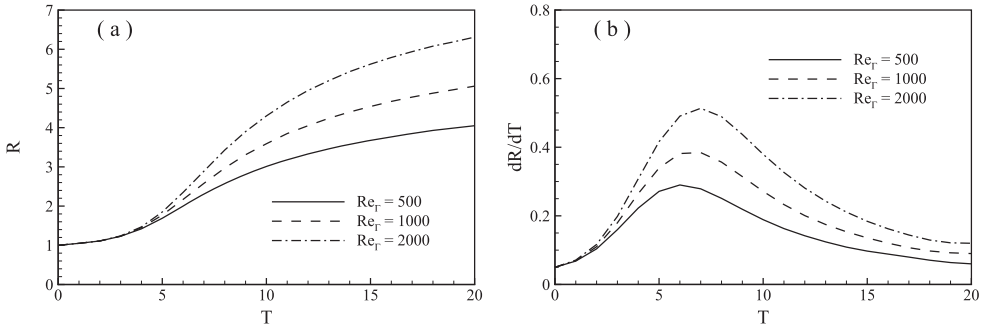

Figure 6. Temporal variation of ring radii and its changed rate at different Re_Γ.

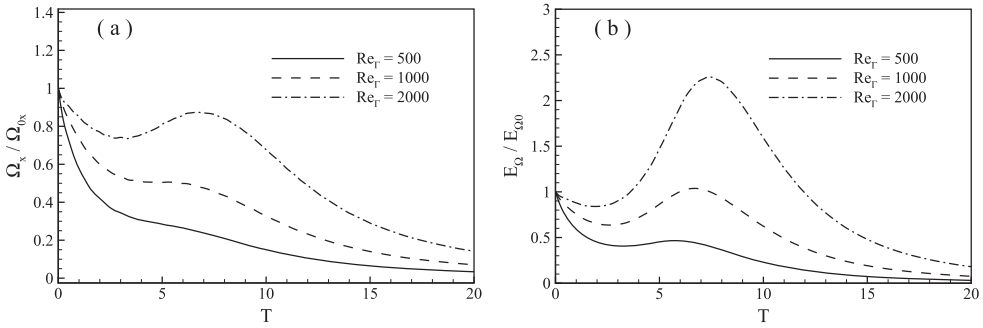

Figure 7. Temporal variation of vorticity at the core center of ring Ω_x and enstrophy E_Ω at different Re_Γ.

Reynolds number, say 2000, the value of Ω_x decreases initially. This decrease is most likely caused by smearing or smoothening out of the vorticity due to a more dominant effect of viscosity in the early stage of the collision. However, the trend reverses during the rapid radial expansion phase when vortex stretching intensifies vorticity in the core, thus causing Ω_x to increases rapidly. After reaching a peak value, Ω_x decreases gradually due to cross diffusion of vorticity of opposite sign as mentioned earlier. Similar variation is observed for the two lower Reynolds numbers cases except that lower Reynolds number leads to lower peak core vorticity value which is in line with the lower rate of radial expansion. As for the temporal variation in enstrophy in the fluid system, the trend follows that of the temporal variation of vorticity except that peak enstrosphy is more distinct.

3.2. Collision between two vortex rings of unequal initial core sizes

To better understand the process of head-on collision between two vortex rings of unequal core sizes, we first examine the self-induced velocity (U_S) of an isolated circular vortex ring, and the induced velocity of one ring on another ring (U_I). The equations governing these two velocities are expressed as follow (Saffman 1970)

$$U_S = \frac{\Gamma}{4\pi R_0}\left[\ln\frac{8R_0}{\sigma_0} - 0.558\right], \tag{10}$$

$$U_I = \frac{\Gamma}{2\pi\sigma}\left[1 - e^{-\left(\frac{\sigma}{\sigma_0}\right)^2}\right], \tag{11}$$

where Γ is circulation of the ring. The above equations indicate that a vortex ring with higher circulation or thinner core size produces higher U_S and U_I. Specifically, when $\sigma_{02} > \sigma_{01}$, or $\Gamma_2 < \Gamma_1$, we have

$$\frac{U_{I2}}{U_{I1}} > 1, \frac{U_{S1}}{U_{S2}} > 1, \tag{12}$$

and as the rings approach in closed proximity

$$\|\mathbf{U}_{I1} + \mathbf{U}_{I2}\| \gg \|\mathbf{U}_{S1} + \mathbf{U}_{S2}\|, \tag{13}$$

where U_{I1} and U_{S1} are the velocity components in the radial and z-directions at the core center of vortex ring 1. Explicitly, U_{I1} is the velocity induced on 'vortex ring 1' by 'vortex ring 2' and U_{S1} is the self-induced velocity of 'vortex ring 1'.

We now discuss the collision between two vortex rings of unequal core sizes with reference to the above equations. These results are presented in figure 8, also in the form of vorticity iso-surfaces, for the core size ratio of $\eta = 1.2$ and 1.5 and fixed Reynolds number 2000. Included in the same figure are the corresponding vorticity contours in the $y = 0$ plane. For purpose of identification, V_1 denotes a thin-core vortex ring (henceforth referred to simply as 'thin-core ring') and V_2 a thick-core vortex ring (henceforth referred to simply as 'thick-core ring'). Despite the unequal core sizes between the two approaching rings, the result depicted in figure 8 shows that the early stage of the collision does not deviate significantly from that of the collision between two identical vortex rings. This is not unexpected since the influence of one ring on the other ring is still small when they are initially far apart. In close-proximity, however, the two rings undergo differential rate of radial expansion because of the differences in their induced velocities on each other. This condition enables the thick-core ring (V_2) to slip-over the thin-core ring (V_1) because of a higher induced velocity on ring V_2 (i.e. U_{I2}). Upon successful slip-over, both the rings contract radially, albeit unequally, as they move away from each other in opposite direction (see figure 8(a) after $T \approx 16$ and figure 8(b) after $T \approx 12$). Figure 8(b) further shows that higher core size ratio (η) enhances the slip-over process and causes a greater reduction of circulation of ring V_2 compared to that of ring V_1. This can be deduced from the relative sizes of their iso-surfaces of constant vorticity, or from their vorticity contours in the $y = 0$ plane. The increased rate of vorticity dissipation of ring (V_2) could be due to the ring undergoing a higher rate of radial expansion and therefore higher vorticity intensification and decay compared to ring (V_1). Inoue *et al* (2000) also observed similar slip-over process during the head-on collision of two circular rings with unequal initial circulations. Unfortunately, they offer no physical explanation for the observed phenomenon. In fact, equations (3.1)–(3.5) clearly show that variation in initial core size has similar effect as variation in initial circulation on the motion of vortex rings.

Figure 9 shows the spatial and temporal variation of the core shape represented by vorticity contour in the upper half of $y = 0$ plane for different η and Re_Γ. As expected, the collision and radial expansion of the rings causes the initial circular vortex core to deform into non-circular shape as their trajectories deviate from the plane of collision. Concurrently, viscous diffusion and cancellation of vorticity of opposite sign reduces the circulation of each ring. The degree of deviation from the collision plane increases with η or with Re_Γ. In the case of low Re_Γ of 500, the lower momentum of the vortex rings and a more dominant effect of viscosity hastens vorticity dissipation and inhibits the slip-over process. On the other hand, slip-over process is achieved at a higher Re_Γ, say 2000 and $\eta \geqslant 1.2$. It is further noted from

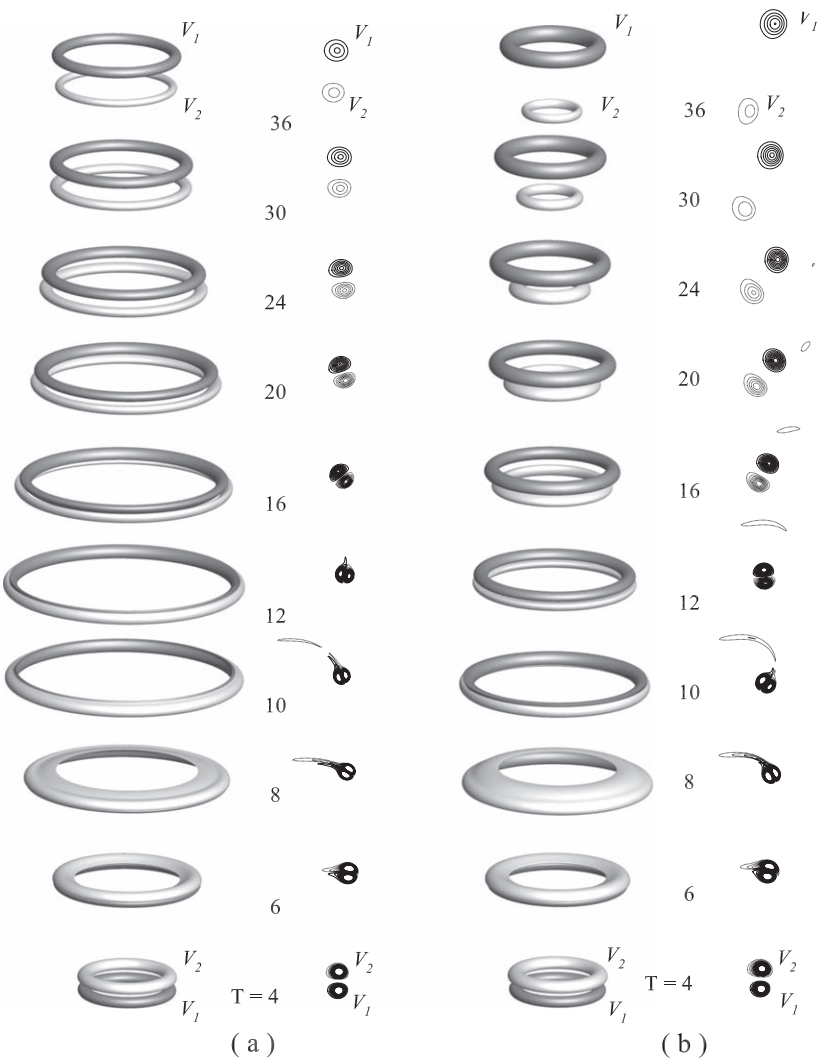

Figure 8. Evolution of vortex rings (represented by the vorticity iso-surface $||\boldsymbol{\Omega}|| = 1.5$) and vorticity contours in the $y = 0$ plane of symmetry for colliding circular rings of unequal initial core size at $Re_\Gamma = 2000$. (Contours are plotted in the range of $|\Omega_y| \leqslant 10$ with a level interval of $\Delta\Omega_y = 0.5$.) (a) $\eta = 1.2$, (b) $\eta = 1.5$.

figure 9 that two vortex rings collide near $z = 0$, and the centers of their vorticities are not on the plane of $z = 0$ when $\eta > 1$.

Figure 10 shows the temporal evolution of vorticity at the core centers on $y = 0$ plane for different core size ratios and Reynolds numbers. When $Re_\Gamma = 500$ (see figure 10(a)), the effect of η on the core vorticity of ring V_1 is not significantly different from that of the collision between identical vortex rings. In contrast, η has considerably more influence on the core vorticity of ring V_2. Take the case of $\eta = 1.5$ as example (see also bottom rightmost result of figure 10), when the two rings first approach each other (up to $T \approx 3$), ring V_2 has less vorticity dissipation compared to that of their equal core size counterpart. This could be attributed to lower radial expansion and therefore less vorticity dissipation at high η (see also

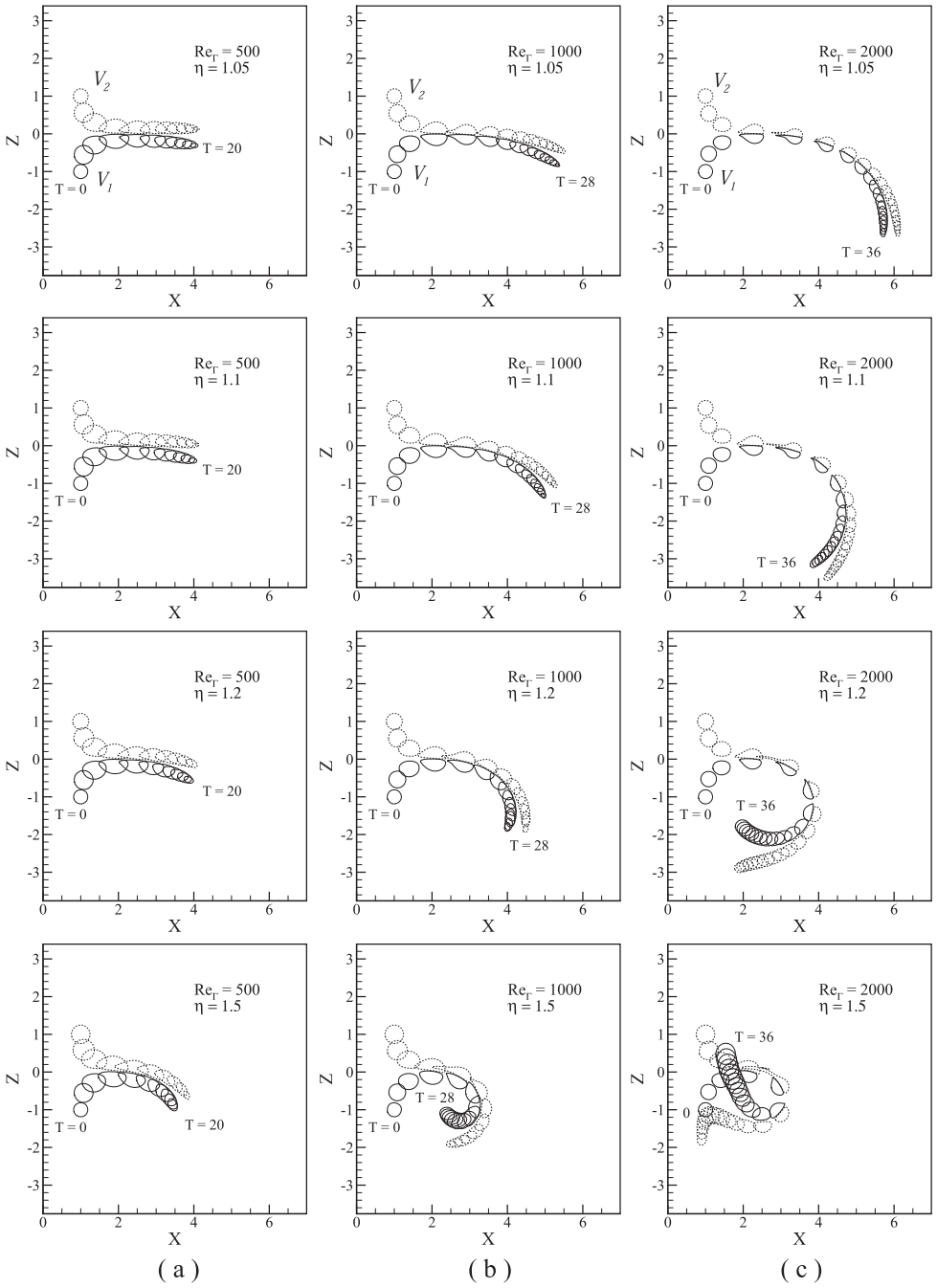

Figure 9. Vorticity contours ($\Omega_y = \pm 1.0$) in the $y = 0$ plane at different Re_Γ and η. (a) $Re_\Gamma = 500$, (b) $Re_\Gamma = 1000$, (c) $Re_\Gamma = 2000$.

the differential rate of radial expansion depicted in figures 8(a) and (b) for two different η at the same Reynolds number). When the rings are in closer proximity, vorticity intensifies ($5 < T < 7$) and the unsuccessful attempt by V_2 to slip-over V_1 (see the bottom frame of

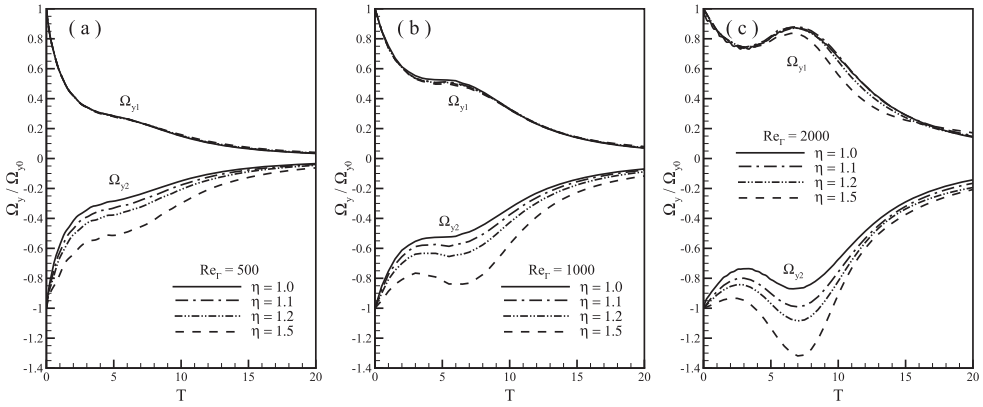

Figure 10. Temporal evolution of vorticity at the core centers in the symmetry plane $y = 0$ for different η and Re_Γ. (a) $Re_\Gamma = 500$, (b) $Re_\Gamma = 1000$, (c) $Re_\Gamma = 2000$.

figure 9(a)) leads to viscous diffusion at the region of contact, thus lowering the vorticity (see figure 10). Lowering the core size ratio (η) of the rings produces similar behavior for ring V_2 except for higher vorticity dissipation at lower (η). Also, there is less deviation of core trajectories from the collision plane compared to their equal core size counterpart. At higher Reynolds number, the influence of core size ratio on both the vortex rings increases, although considerably more so on ring V_2. Take the case of $Re_\Gamma = 1000$ and $\eta = 1.5$ as an example, while the rate of radial expansion for the two rings is higher than their lower Reynolds number counterpart, ring V_2 is subjected to a higher rate of radial expansion than V_1, thus generating a local peak vorticity at $T \approx 6$. Thereafter, the vorticity reduces monotonically as viscous diffusion dominates. At this Reynolds number, it can also be observed that the thick-core ring V_2 has successfully slipped over the thin-core ring V_1 for $\eta = 1.5$ (see figure 9(b)), and the behavior of vortex rings thereafter is similar as that discussed earlier, except that vorticity dissipation extends over a longer period compared to lower η cases at the same Reynolds number. For even higher Reynolds number of $Re_\Gamma = 2000$, the vorticity distribution broadly displays similar trend as before except that the rate of radial expansion is higher during the early stages of interaction and rate of vorticity dissipation is lower during the later stages of interaction.

Figure 11 shows the temporal variation of KE E_u and enstrophy E_Ω as a function of Re_Γ and η. In all the cases considered here, higher η lessens the rate of KE reduction and reduces vorticity dissipation. As for the enstrophy, the trend mirrors that of the variation of vorticity (see figure 10), i.e. higher vorticity results in higher enstrophy. Likewise, higher Reynolds number increases the rate of radial expansion and therefore higher vorticity intensification and higher enstrophy as can be seen in figure 11(d).

3.3. Azimuthal instability

It is well known that an isolated vortex ring can develop an azimuthal instability under some circumstance, and this instability can affect its subsequent motion and its interaction with another vortex ring, such as head-on collision of two identical vortex rings as was briefly discussed in the code validation. Here, we examine how the azimuthal instability affect the outcome of the same head-on collision when their vortex core sizes are no longer equal. To do this, the vorticity of each ring is perturbed in the azimuthal direction by displacing the axis of the vortex core using a sine-wave perturbation (Verzicco and Orlandi 1994, Mansfield

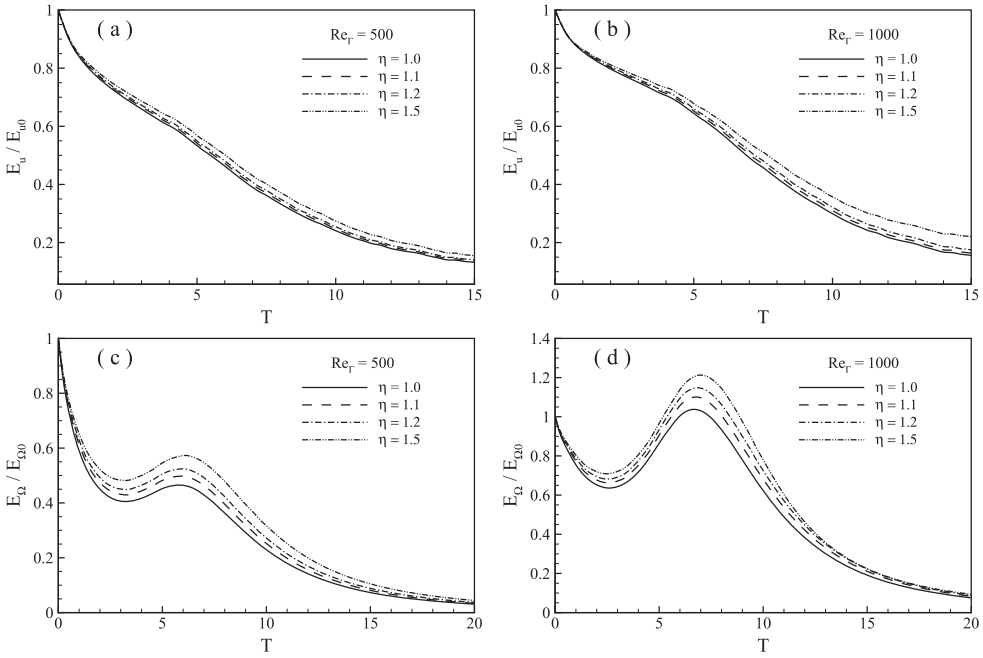

Figure 11. Temporal variation of kinetic energy E_u and enstrophy E_Ω for different Re_Γ and η. (a) $Re_\Gamma = 500$, (b) $Re_\Gamma = 1000$, (c) $Re_\Gamma = 500$, (d) $Re_\Gamma = 1000$.

et al 1999, Cheng *et al* 2016), and the results of the collision are presented in the following section.

For purpose of comparison, the results for the collision between two vortex rings with equal core size (i.e. identical rings) are also presented here. First, we examine if perturbation amplitudes A_m affect the overall collision process before discussing specific cases. To do this, we impose a fixed azimuthal wavenumber of $N = 15$ on approaching vortex rings. The wavenumber adopted is within the range of perturbation parameter $15 \leqslant N \leqslant 20$ observed in experiments (Lim and Nickels 1992) and in the model prediction for counter-rotating trailing vortices (Crow 1970). Figure 12 shows the vorticity contours in the $z = 0$ plane for different Re_Γ and A_m at a selected time instant of $T = 40$. The results show that when two identical vortex rings of low Reynolds number are forced to collide head-on, the dominate effect of viscosity hasten their vorticity decay and inhibit vortex reconnection. This applies to all perturbation amplitudes considered as can be seen in figures 12(a)–(c) for the case of $Re_\Gamma = 600$. However, at a moderate Reynolds number, vortex reconnection takes place at the regions of contact between the perturbed vortex filaments, and this leads to the generation of vortex ringlets as discussed previously (see figures 12(d)–(f) $Re_\Gamma = 800$). Since our simulation shows that the inclusion of azimuthal perturbations does not significantly affect the early stage of the collision although higher A_m brings about earlier reconnection at a later stage of the collision, we decided to fix $A_m = 0.05$ for all subsequent computation unless otherwise stated.

Results of the temporal variation of KE and enstrophy during various stages of collision are presented in figure 13 for different perturbation amplitudes at two predetermined Reynolds number of $Re_\Gamma = 600$ and $Re_\Gamma = 800$; the rest of the flow conditions are fixed and identical to those in figure 12. Interestingly, figure 13 shows that for a fixed Reynolds

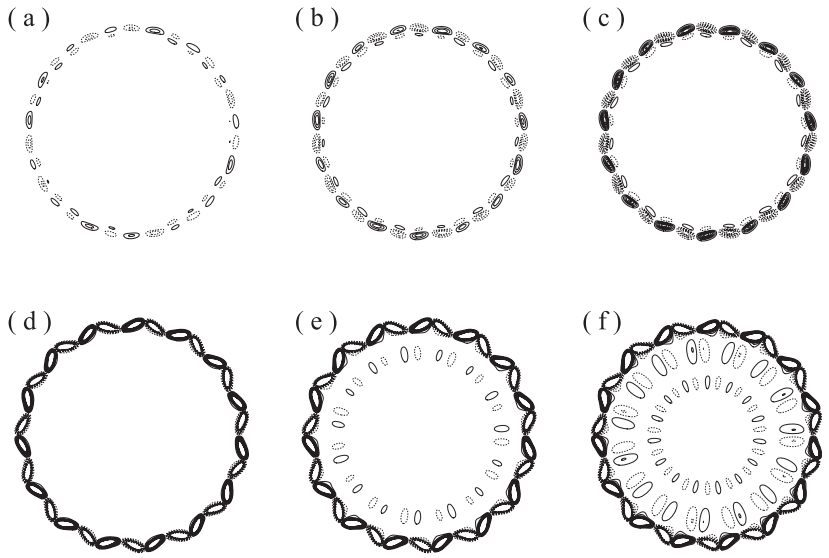

Figure 12. The vorticity contours pattern in the $z = 0$ plane in the case of $N = 15$ and $\sigma_{01} = \sigma_{02} = 0.1R_0$ at different Re_Γ and $T = 40$. (a) $Re_\Omega = 600$, $A_m = 0.02$ (b) $Re_\Gamma = 600$, $A_m = 0.03$, (c) $Re_\Gamma = 600$, $A_m = 0.05$, (d) $Re_\Gamma = 800$, $A_m = 0.02$ (e) $Re_\Gamma = 800$, $A_m = 0.03$, (f) $Re_\Gamma = 800$, $A_m = 0.05$.

number, varying the perturbation amplitude does not significantly affect the KE of the fluid system, although it has a noticeable effect on E_Ω (see figure 13(b)). To better understand this behavior, we first take a closer look at the case of $Re_\Gamma = 800$. The results show that, regardless of A_m, the enstrophy initially decreases at approximately the same rate until $T = 1$. This initial decay can be attributed to vorticity decay by viscous diffusion when mutual interaction between the two rings is minimal at this early stage. After $T = 1$, the rate of decay begins to deviate from each other although they all continue their downward trends until $T = 3$. This deviation in the results at $T = 1$ is likely due to the growth of azimuthal perturbation, and higher A_m causes a higher rate of enstrophy reduction. In all cases, the downward trend reverses after $T = 3$. This rise in enstrophy can be attributed to radial expansion or stretching of vortex rings during the collision and leads to vorticity intensification. After reaching a peak value at $T = 6$, the enstrophy decreases; at first rapidly and then gradually. The rapid reduction is likely to be due to the generation vortex ringlets and the subsequent more gradual decay could be due to viscous diffusion as these ringlets propagate away through self-induction. This same trend is observed in all perturbation amplitudes although higher initial A_m produces lower overall enstrophy (see figure 13(d)). Obviously, a lower Reynolds number (i.e. $Re_\Gamma = 600$) for a fixed perturbation amplitude leads to lower enstrophy. It is worth noting that, the number of vortex ringlets depicted in the figures is dictated by the predetermined wavenumber (N) of the azimuthal perturbation, as is clearly demonstrated in figure 14 for three different wave numbers at a selected time instant of $T = 20$ and $Re_\Gamma = 1500$. Obviously, in the real flow situation the number of vortex ringlets is governed by the azimuthal instability of the vortex filaments which is beyond the scope of this study.

When vortex core sizes of the two colliding rings are no longer equal, the outcomes of the collision change significantly. Their changes are affected by not only the ratio of vortex core size, but also the Reynolds number of the approaching rings and the imposed initial

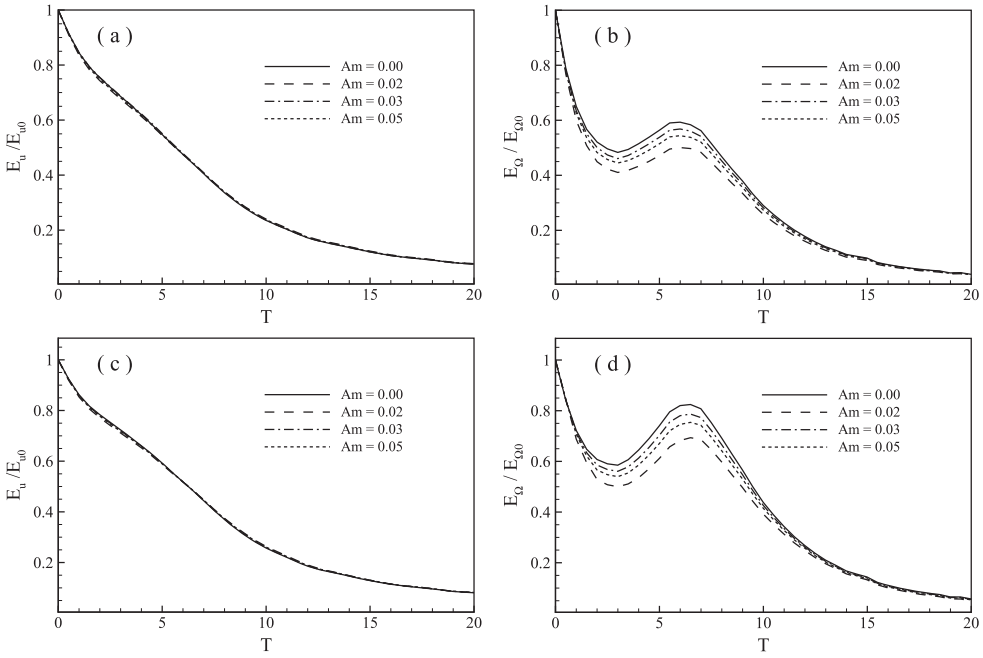

Figure 13. Temporal variation of kinetic energy E_u and enstrophy E_Ω for different A_m and Re_Γ. (a) and (b) $Re_\Omega = 600$, (c) and (d) $Re_\Gamma = 800$.

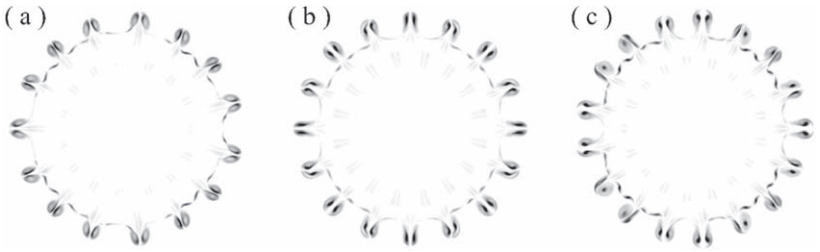

Figure 14. Dependence of the vorticity contours in the $z = 0$ plane on the wavenumber N for $Re_\Gamma = 1500$ and $\sigma_{01} = \sigma_{02} = 0.1R_0$ at $T = 20$. (a) $N = 15$, (b) $N = 16$, (c) $N = 17$.

azimuthal perturbation amplitude A_m. For specific cases of fixed perturbation amplitude and Reynolds number ($Re_\Gamma = 1200$), the influence of the core size ratio on the evolution of the colliding rings are presented in figure 15 for $\eta = 1.1$, 1.2 and 1.5. In all these cases, the attempt by ring V_2 (thick-core ring) to slip over ring V_1 (thin-core ring) results in a re-alignment of their azimuthal perturbations and a re-orientation of resulting vortex ringlets that are no longer propagating radially outward from the center of the primary rings. Instead, they travel at an angular offset (on the average) to the collision plane, with higher core size ratio produces higher inclination angle. Concurrent to the production of vortex ringlets, segments of the stretched vortex filaments are left behind in the form of vortex loops which are distributed around the circumference of the 'remnant' primary vortex rings. Eventually, both the vortex loops and the vortex ringlets are dissipated through viscous diffusion. A more

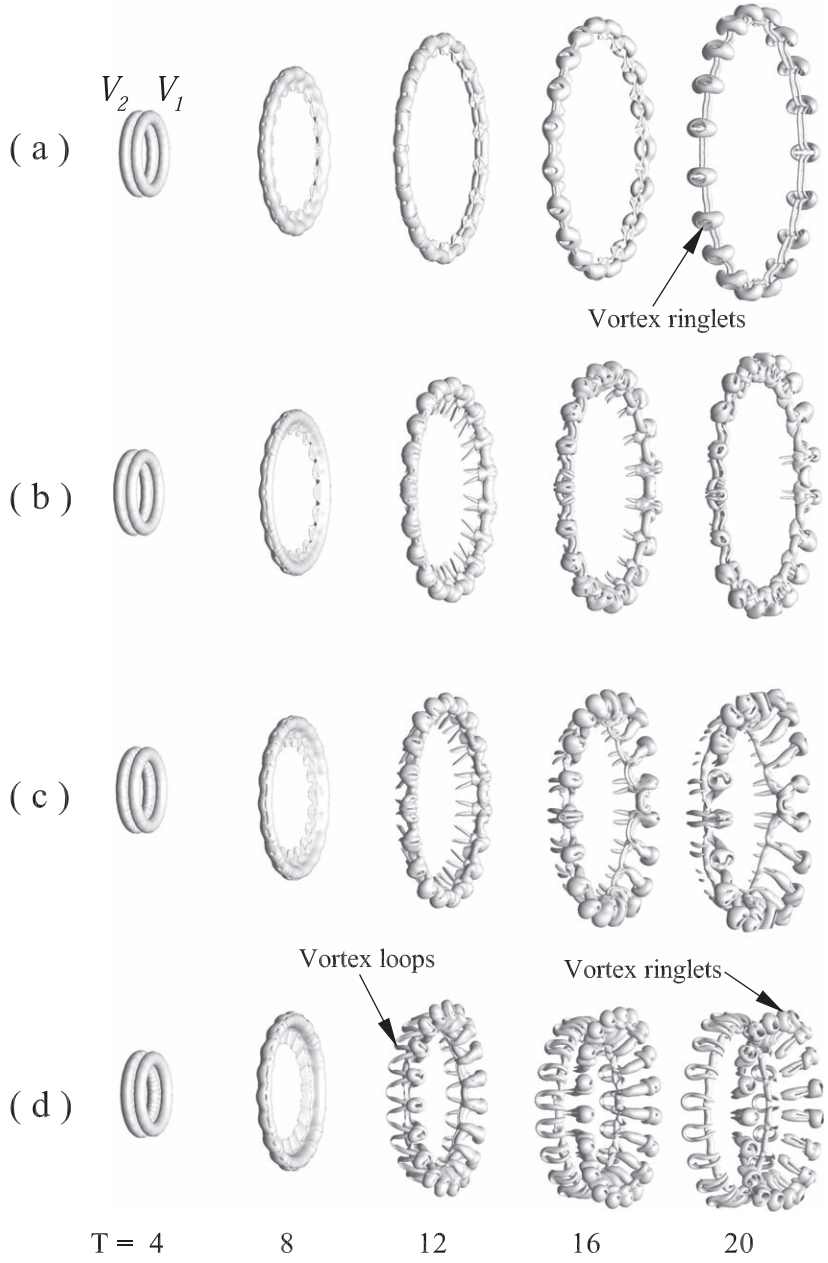

Figure 15. Vortex structure patterns (represented by the iso-surface of a constant vorticity $||\boldsymbol{\Omega}|| = 1$) for $Re_\Gamma = 1200$ and $N = 19$ at different η and times. (a) $\eta = 1$, (b) $\eta = 1.1$, (c) $\eta = 1.2$, (d) $\eta = 1.5$. Note that vortex ringlets are propagating outward at an angle to the collision plane.

distinct formation of vortex ringlets and vortex loops is depicted in figure 16, where the colliding vortex rings are zoomed in to show the evolution of vortex ring filaments during the slip-over process in figure 15(d). Figure 17 shows the authors' interpretation of how these

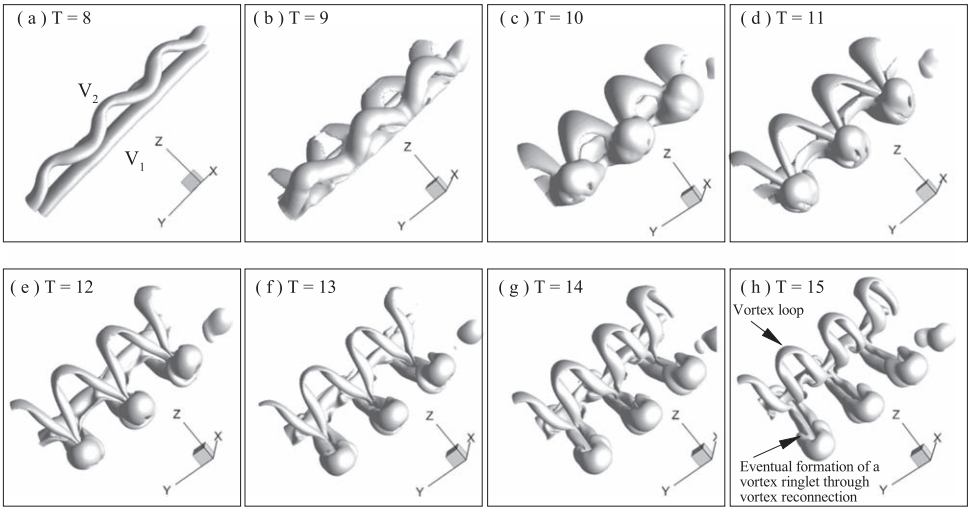

Figure 16. Close-up view showing the evolution of vortex ring filaments during the slip-over process for the case $Re_\Gamma = 1200$, $N = 19$ and $\eta = 1.5$. Except for (a) and (b) which respectively have a contour level of $||\boldsymbol{\Omega}|| = 8$ and 4 to accentuate the vortex filaments, (g) and (h) have a contour level of $||\boldsymbol{\Omega}|| = 1.0$, the other parts (c)–(f) have a contour level of $||\boldsymbol{\Omega}|| = 1.5$.

vortex ringlets and vortex loops are generated. For the sake of clarity, the curved filaments of the vortex rings are replaced by straight vortex filaments. Here, when the two approaching vortex rings are in proximity to each other, the higher induced velocity field produced by the thin cored vortex ring may have contributed to an early development of an azimuthal instability on the thick cored vortex ring, while the reverse effect (i.e. the influence of the thick cored ring on the thin cored ring) is muted (see figure 17(b)). The instability grows spatially with time, and as the thick cored ring attempts to slip over the thin cored ring, the upstream portion of the instability develops a 'kink'; due to the mutual induction. This kink amplifies and causes the vortex filaments to come together, and at where they touch, vortex reconnection takes place between them and leads to the eventual formation of vortex ringlet. Concurrently, the remaining parts of the vortex filaments within a rectangular italic C (see figure 17(e)) are entrained by the induced velocity of the thin cored ring. This action, together with the self-induction of the ringlet causes the connecting vortex filaments to the ringlet to stretch and eventually dissipate via viscous diffusion, while the downstream part of the azimuthal instabilities of the thick cored vortex ring transforms into a vortex loop as can be seen in figure 17(f). The authors believe that the above mentioned process of ringlet and vortex loop formation also applies to colliding vortex rings with lower circulation and core size ratio as can be seen in figures 15(b) and (c) although the vortex loops are less distinct than those in figure 15(d). It is worth noting that the 'discontinuity' in the vortex loops in figures 15(b) and (c) is due to vorticity of the loops in those regions lower than the present threshold value. As for the associated temporal variations of KE E_u and enstrophy E_Ω for the collision of unequal core sizes, they are plotted as shown in figure 18 for different η. Similar to the collision of two identical vortex rings, the results show E_u is affected significantly less by changes in η than E_Ω, and in both cases, higher η produces higher E_u and E_Ω.

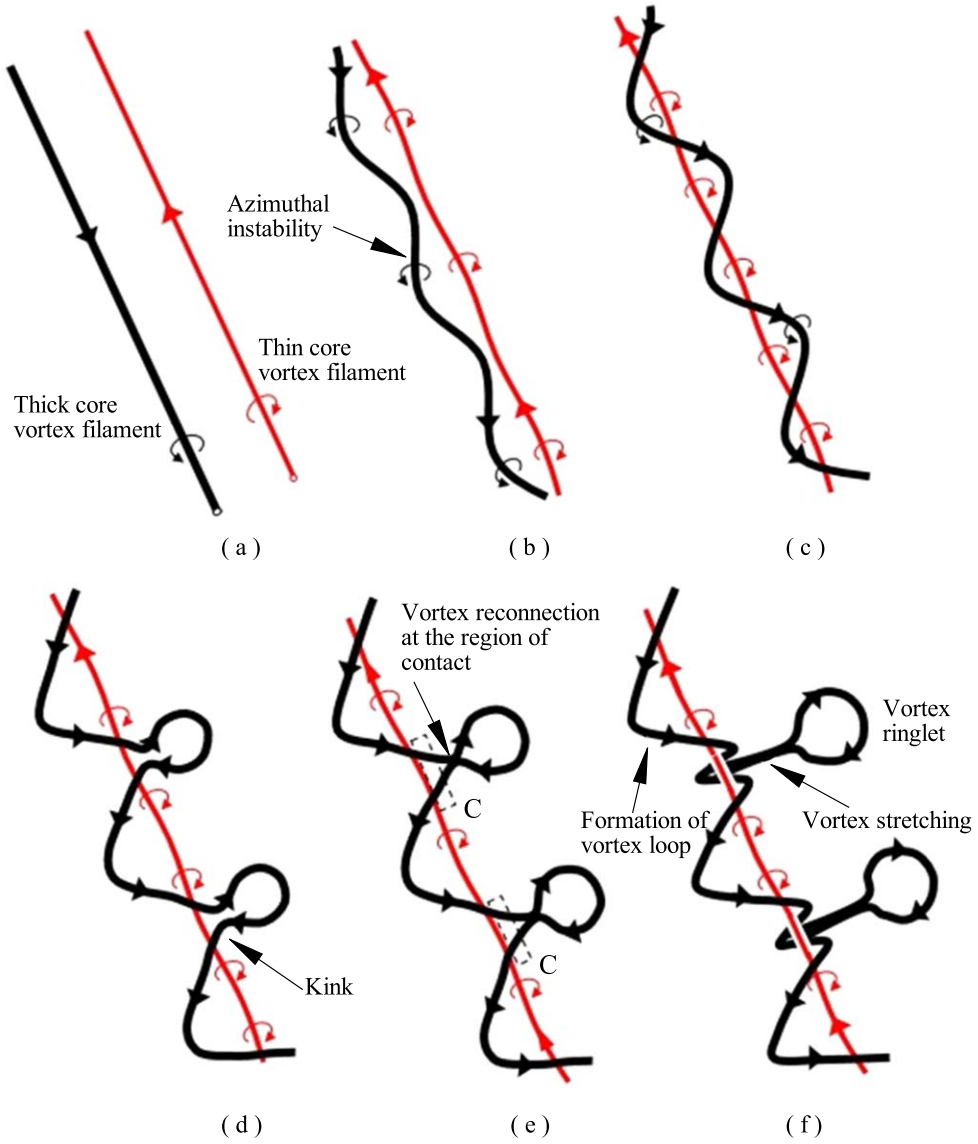

Figure 17. Authors' interpretation of the process leading to the generation of vortex ringlets and vortex loops during the head-on collision of two vortex rings of unequal core sizes. For the sake of clarity and easy comprehension, the curved filaments of the vortex rings are replaced by straight vortex filaments. An arrow head on each vortex filament indicates the direction of vorticity vector.

4. Conclusion

Head-on collision of two viscous circular vortex rings of unequal core sizes has been investigated numerically using the LBM for a range of Reynolds numbers (Re_Γ) and core size ratios (η). Our results show that dissimilarity in vortex core sizes between the two colliding vortex rings can significantly alter the outcomes of the collision. Unlike the collision between two identical vortex rings where symmetrical condition exists (at least in the early stage of the

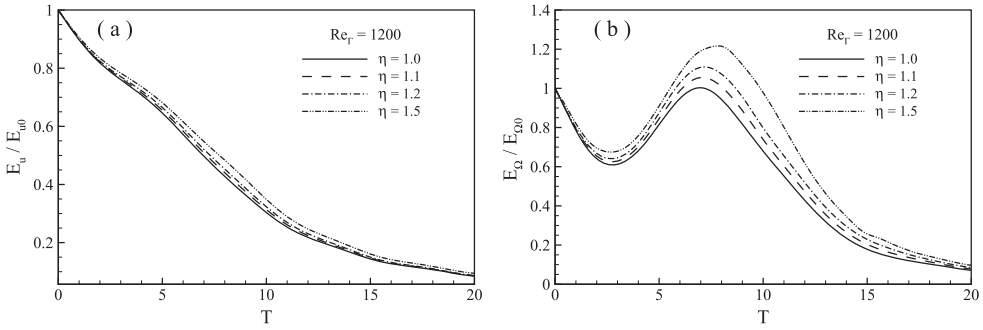

Figure 18. Temporal variation of kinetic energy E_u and enstrophy E_Ω for different η at $Re_\Gamma = 1200$ and $N = 19$.

collision), here, unequal core size induces unequal velocities on each other, which leads to unequal rate of radial expansion between the two rings. This behavior sets up a scenario where the thick-core (slower moving) vortex ring can slip-over a thin-core (faster moving) vortex ring if the Reynolds number is sufficiently high. After the slip-over, the two rings contract radially, albeit unequally, due to mutual induction as they travel away from each other in opposite direction. For vortex rings of sufficiently low Reynolds number, the lower momentum of the vortex rings, couples with a more dominant effect of viscosity inhibits a successful slip-over process. In which case, the two vortex rings remain in constant proximity throughout the interaction, and this leads to their eventual 'demise' due to cross diffusion of vorticity of opposite sign at the regions of contact. In the presence of azimuthal perturbations for the case of moderately high Reynolds number vortex rings, an attempt by a thick-core ring to slip-over a thin-core ring results in a re-alignment of azimuthal perturbations between the two rings, leading to the generation of vortex ringlets that are no longer propagating radially outward from the centers of the primary rings. Instead they travel in directions that are inclined to the plane of collision, and the inclination angle increases with core radius ratio (η). For the low Reynolds number counterpart, the dominate effect of viscosity inhibit vortex reconnection of azimuthal perturbation, and the close-proximity of the two rings eventually leads their 'demise'. An important outcome of the present study is that variation in vortex core sizes between two colliding vortex rings does affect the outcome of the collision, especially at moderate Reynolds numbers. This may partly help to explain the inconsistency in some of the experimental observations, although imprecise alignment of the two approaching vortex rings and variation in their circulation may also play a part. The latter factor is not considered here as variation in the circulation of two colliding rings also results in variation in their Reynolds number which further complicates the matter.

Acknowledgments

This work was supported by the A*STAR Computational Resource Center through the use of its high performance computing facilities.

ORCID iDs

M Cheng https://orcid.org/0000-0002-6713-966X

References

Bergdorf M, Koumoutsakos P and Leonard A 2007 Direct numerical simulations of vortex rings at $Re_\Gamma = 7500$ *J. Fluid Mech.* **581** 495–505

Borisov A V, Kilin A A, Mamaev I S and Tenenev V A 2014 The dynamics of vortex rings: leapfrogging in an ideal and viscous fluid *Fluids Dyn. Res.* **46** 031415

Bourne K, Wahono S and Ooi A 2017 Numerical investigation of vortex ring ground plane interactions *J. Fluids Eng.* **139** 071105

Cheng M, Lou J and Lim T T 2014 A numerical study of a vortex ring impacting a permeable wall *Phys. Fluids* **26** 103602

Cheng M, Lou J and Lim T T 2015 Leapfrogging of multiple coaxial voscous vortex rings *Phys. Fluids* **27** 031702

Cheng M, Lou J and Lim T T 2016 Evolution of an elliptic ring in a viscous fluid *Phys. Fluids* **28** 037104

Cheng M, Lou J and Luo L S 2010 Numerical study of a vortex ring impacting a flat wall *J. Fluid Mech.* **660** 430–55

Cheng M and Luo L S 2007 Charactristics of two-dimensional flow around a rotating circular cylinder near a plane wall *Phys. Fluids* **19** 063601

Chen S and Doolen G D 1998 Lattice Boltzmann method for fluid flows *Annu. Rev. Fluid Mech.* **30** 329–64

Chu C C, Wang C T, Chang C C, Chang R Y and Chang W T 1995 Head-on collision of two coaxial vortex rings: experiment and computation *J. Fluid Mech.* **296** 39–71

Crow S C 1970 Stability theory for a pair of trailing vortices *AIAA J.* **8** 2172–9

Guan H, Wei Z J, Rasolkova E R and Wu C J 2016 Numerical simulation of two coaxial vortex rings head-on collision *Adv. Appl. Math. Mech.* **8** 616–47

Gurzhii A A and Konstantinov M Y 1989 Head-on collision of two coaxial vortex rings in an ideal fluid *Fluid Dyn.* **24** 538–41

Inoue O, Hattori Y and Sasaki T 2000 Sound generation by coaxial collision of two vortex rings *J. Fluid Mech.* **424** 327–65

Junk M 2001 A finite difference interpretation of the lattice Boltzmann method *Numer. Methods Part. Differ. Equ.* **17** 383–402

Kelso R M, Lim T T and Perry A E 1996 An experimental study of round jets in a cross-flow *J. Fluid Mech.* **306** 111–44

Konstantinov M Y 1994 Chaotic phenomena in the interaction of vortex rings *Phys. Fluids* **6** 1752–67

Lim T T 1997a On the role of Kelvin–Helmholtz-like instability in the formation of turbulent vortex rings *Fluid Dyn. Res.* **21** 47–56

Lim T T 1997b A note on the leapfrogging between two coaxial vortex rings at low Reynolds numbers *Phys. Fluids* **9** 239–41

Lim T T 1998 On the breakdown of vortex rings from inclined nozzles *Phys. Fluids* **10** 1666–71

Lim T T and Nickels T B 1992 Instability and reconnection in the head-on collision of two vortex rings *Nature* **357** 225–7

Lim T T and Nickels T B 1995 *Vortex Rings, in Fluid Vortices* ed S I Green (Dordrecht: Kluwer)

Lugt H J 1983 *Vortex Flow in Nature and Technology* (New York: Wiley)

Mansfield J R, Knio O M and Meneveau C 1999 Dynamic les of colliding vortex rings using a 3d vortex method *J. Comput. Phys.* **152** 305–45

Mariani R and Kontis K 2010 Experimental studies on coaxial vortex loops *Phys. Fluids* **22** 126102

Meleshko V V 2010 Coaxial axisymmetric vortex rings: 150 years after helmholtz *Theor. Comput. Fluid Dyn.* **24** 403–31

Orlandi P and Verzicco R 1993 Vortex rings impinging on walls: axisymmetric and three-dimensional simulations *J. Fluid Mech.* **256** 615–46

Oshima Y 1978 Head-on collisiion of two vortex rings *J. Phys. Soc. Japan* **44** 328–31

Pullin D I and Saffman P G 1998 Vortex dynamics in turbulence *Annu. Rev. Fluid Mech.* **30** 31–51

Saffman P G 1970 The velocity of viscous vortex rings *Stud. Appl. Math.* **49** 371–9

Saffman P G 1992 *Vortex Dynamics* (Great Britain: Cambridge University Press)

Shariff K and Leonard A 1992 Vortex rings *Annu. Rev. Fluid Mech.* **24** 235–79

Stanaway S, Shariff K and Hussain F 1988 Head-on collision of viscous vortex rings *Proc. Summer Program, Center for Turbilence Research* pp 287–309

Verzicco R and Orlandi P 1994 Normal and oblique collisions of a vortex ring with a wall *Meccanica* **29** 383–91
Widnall S E, Bliss D B and Tsai C 1974 The stability of short waves on a vortex ring *J. Fluid Mech.* **66** 35–47
Widnall S E and Sullivan J P 1973 On the stability of vortex rings *Proc. R. Soc.* A **332** 335–53
Yamada H and Matsui T 1978 Preliminary study of mutual slip-through of a pair of vortices *Phys. Fluids* **21** 292–4